Development of a Large Animal Model of Osteochondritis Dissecans of the Knee

A Pilot Study

Christian G. Pfeifer,*† MD, Stuart D. Kinsella,*† MD, Andrew H. Milby,*† MD, Matthew B. Fisher,*† PhD, Nicole S. Belkin,*† MD, Robert L. Mauck,*†‡ PhD, and James L. Carey,*†§ MD, MPH

Investigation performed at the McKay Orthopaedic Research Laboratory, University of Pennsylvania, Philadelphia, Pennsylvania, USA

Background: Treatment of osteochondritis dissecans (OCD) of the knee is challenging, and evidence for stage-dependent treatment options is lacking. Basic science approaches utilizing animal models have provided insight into the etiology of OCD but have yet to produce a reliable and reproducible large animal model of the disease on which to test new surgical strategies.

Purpose/Hypotheses: The purpose of this study was to develop an animal model featuring an OCD-like lesion in terms of size, location, and International Cartilage Repair Society (ICRS) grading. The hypothesis was that surgical creation of an osteochondral defect followed by placement of a barrier between parent bone and progeny fragment would generate a reproducible OCD-like lesion.

Study Design: Controlled laboratory study.

Methods: Bilateral osteochondral lesions were created in the medial femoral condyles of 9 Yucatan minipigs. After lesion creation, a biodegradable membrane was interposed between the progeny and parent bone. Five different treatment groups were evaluated at 2 weeks: a control with no membrane (ctrl group; n = 4), a slowly degrading nanofibrous poly(ε-caprolactone) membrane (PCL group; n = 4), a fenestrated PCL membrane with 1.5-mm holes covering 25% of surface area (fenPCL group; n = 4), a collagen membrane (Bio-Gide) (CM group; n = 3), and a fenestrated CM (fenCM group; n = 3). Five unperturbed lateral condyles (1 from each treatment group) served as sham controls. After euthanasia on day 14, the lesion was evaluated by gross inspection, fluoroscopy, micro–computed tomography (micro-CT), and histology. To quantify changes between groups, a scoring system based on gross appearance (0-2), fluoroscopy (0-2), and micro-CT (0-6) was established. Micro-CT was used to quantify bone volume per total volume (BV/TV) in a defined region surrounding and inclusive of the defect.

Results: The no scaffold group showed healing of the subchondral bone at 2 weeks, with continuity of subchondral bone elements. Conversely, condyles treated with PCL or CM showed substantial remodeling, with loss of bone in both the progeny fragment and surrounding parent bone. When these membranes were fenestrated (fenPCL and fenCM groups), bone loss was less severe. Histological analysis showed no integration in the cartilage layer in any treatment group, while fibrous tissue formed between the parent and progeny fragments. Micro-CT showed significant differences in mean BV/TV between the PCL (27.4% ± 2.3%) and the sham (47.7% ± 1.4%) or no scaffold (54.9% ± 15.1%) groups ($P < .01$ and $P < .05$, respectively). In addition, a significant difference in bone loss was evident between the PCL and fenPCL groups (mean BV/TV, 46.6% ± 15.2%; $P < .05$), as well as between the PCL and fenCM (mean BV/TV, 50.9% ± 3.5%) and fenPCL groups ($P < .01$). Grading by 6 blinded reviewers using an OCD scoring system with 3 subcategories showed a significant difference between control and PCL groups.

Conclusion: This study successfully developed a large animal model of OCD-like lesions in the knee joint of Yucatan minipigs. The lesions generated matched characteristics of an ICRS grade 3 OCD lesion in humans. These findings set the stage for ongoing model refinement as well as exploration of novel interventional therapies to restore function and bone and cartilage patency in individuals affected by this rare but significant disease.

Clinical Relevance: This developed model will serve as a platform on which to further investigate the natural course as well as emerging treatment options for OCD.

Keywords: Knee; osteochondritis dissecans; biology of bone; biology of cartilage; tissue engineering

The Orthopaedic Journal of Sports Medicine, 3(2), 2325967115570019
DOI: 10.1177/2325967115570019

Osteochondritis dissecans (OCD) is a disorder of subchondral bone and associated articular cartilage that culminates in the physical separation of a segment of subchondral bone and attached articular cartilage (progeny fragment) from the surrounding bone and cartilage (parent).[1] The most common location for OCD lesions is the knee, with the "classic location" being the lateral aspect of the medial femoral condyle.[2,32] Though incidence is low, ranging from 0.03% to 1.2%,[4,23] the disease is most often diagnosed in patients between 10 and 15 years of age.[12] OCD is therefore significant in that long-term consequences include debilitating degenerative joint disease, sometimes resulting in total knee arthroplasty at a young age. As such, the impact of improved treatments for OCD lesions is tremendous. To make such progress, however, additional studies are required to understand the etiology of the disease and to assess the results of surgical repair.

To date, the etiology of OCD remains unknown. Though originally described by König[22] in 1888 as an inflammatory process leading to necrosis, no inflammatory cells have been observed in histological studies.[18,27,34,35] Some studies impress the importance of an initial change in the subchondral bone involving bone necrosis or trauma, followed by abnormal remodeling.[38] The common presentation of OCD in weightbearing portions of the joint and the increased prevalence in highly active patients[8] support the notion of repetitive microtrauma playing a role. Indeed, mechanical axis malalignment may be associated with OCD development,[19] and lesions appear most commonly in areas of greatest pressure.[7] Ischemia also appears to play a role; clinical data shows evidence of vascular insufficiency within lesions,[26] and in animal models, OCD-like lesions can be instigated by interruption of vascularity in the secondary centers of ossification during development.[28] Additionally, the findings of familial OCD, and more recently, abnormal extracellular matrix components in these affected individuals, highlight a potential genetic component to the disease.[31,36] Though the etiology of the disease has not been fully worked out, it is likely multifactorial, involving vascular insufficiency, a genetic predisposition, necrosis, and repetitive microtrauma.[3,15,32,33,40]

There exists considerable debate as to the best course of management of OCD, an issue complicated by the spectrum of disease presentation and lesion stability. The recent American Academy of Orthopaedic Surgeons (AAOS) clinical practice guideline reflects the inconclusive evidence,[10] especially in International Cartilage Repair Society (ICRS)[6] grade 3 and 4 lesions that regularly require surgical restoration. Given the relatively low incidence of OCD in humans, however, it is difficult to execute large prospective, randomized clinical trials to compare treatment modalities and their outcomes,[13] and so the field remains split on the best surgical approach.

To address this, a number of groups have investigated OCD lesions in various animal models. OCD occurs in almost every species and is a common cause of musculoskeletal malfunction in animals used in meat production.[16,25,30,42] Investigations in small animals (such as rats and rabbits)[5] as well as in pigs and horses[9,28] have shown that perturbation of the cartilage blood supply contributes to the onset of the disease.[41,43] However, these studies have focused primarily on understanding the antecedents of disease, with only 1 study focused on treatment, and then only in a small animal model (rabbit).[24] Development of a reproducible OCD lesion model, in terms of size, location, and grading, in a large animal model would provide a valuable platform by which to test and evaluate treatment options (such as retroarticular and transarticular drilling[17]) as well as to enable the assessment of new treatment strategies.[11] Doing so in a large animal model would further provide biomechanical as well as anatomic features[1] consistent with humans that would enable ready translation of findings to patients.

Toward that goal, we tested the hypothesis that a reproducible OCD-like lesion (representative of an ICRS grade 3 lesion[6]) could be generated in the Yucatan minipig. Here, we hypothesized that if a state of nonunion could be generated between the parent and progeny fragment, a stable fibrous interface might develop. To generate lesions, we created large osteochondral defects on the medial femoral condyle of 9 minipigs. The surgically generated "progeny" fragment was reinserted into the defect with the interposition of membranes of various types (biologic and natural) and porosities (full membranes or with fenestration) to differentially effect healing. Using the "dead in situ" ICRS grade 3 lesion as a benchmark, we evaluated healing of these osteochondral lesions at 2 weeks according to their gross appearance, histological analysis of the parent and progeny interface, and by micro–computed tomography (micro-CT) of the bone quality and healing across the defect. Results of this pilot study show that interposition of a degradable membrane can foster the development of a stable OCD-like lesion, characterized by fibrous nonunion between parent and progeny fragment. These findings set the stage for long-term evaluation of defect progression and the development and evaluation of novel surgical approaches for the treatment of OCD lesions in humans.

§Address correspondence to James L. Carey, MD, MPH, Hospital of the University of Pennsylvania, Penn Sports Medicine Center, Weightman Hall, 1st Floor, 235 South 33rd Street, Philadelphia, PA 19104, USA (email: james.carey@uphs.upenn.edu).

*McKay Orthopaedic Research Laboratory, Department of Orthopaedic Surgery, Perelman School of Medicine, University of Pennsylvania, Philadelphia, Pennsylvania, USA.

†Translational Musculoskeletal Research Center, Philadelphia VA Medical Center, Philadelphia, Pennsylvania, USA.

‡Department of Bioengineering, University of Pennsylvania, Philadelphia, Pennsylvania, USA.

C.G.P. and S.D.K. contributed equally to this article.

One or more of the authors has declared the following potential conflict of interest or source of funding: This work was supported by the National Institutes of Health via a pilot grant from the Penn Center for Musculoskeletal Disorders (Grant P30-AR050950-07). Additional funding was provided by the Department of Orthopaedic Surgery at the Perelman School of Medicine at the University of Pennsylvania, as well as a research fellowship from the Deutsche Forschungsgemeinschaft (German Research Foundation) to C.G.P. (PF 804/1-1). All animal surgeries were performed at the Philadelphia VA Medical Center.

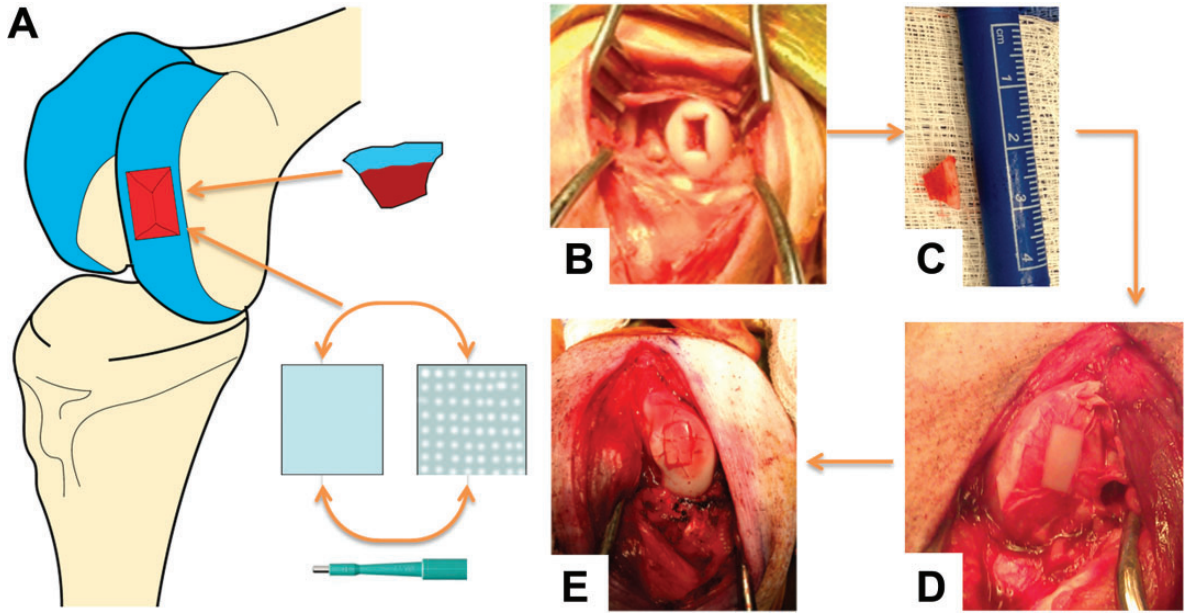

Figure 1. Surgical overview. (A) Schematic representation of the surgery. Osteochondral defect creation on the lateral aspect of the medial femoral condyle and placement of a nonfenestrated or fenestrated scaffold at the interface between the parent bone and progeny fragment. (B) Gross intraoperative picture of the surgical exposure and defect creation in the medial femoral condyle. (C) Typical progeny fragment. (D) Intraoperative image of progeny fragment placed back into defect with a nanofibrous poly(ε-caprolactone) (PCL) membrane (nonfenestrated, untrimmed) in place. (E) Intraoperative image of progeny fragment sutured in place after trimming excess membrane.

MATERIALS AND METHODS

Scaffold Selection and Preparation

Two different classes of membranes were selected to provide semipermeable barriers to regulate the healing of osteochondral defects. The first was a slowly degrading nanofibrous poly(ε-caprolactone) (PCL) membrane fabricated by electrospinning. These membranes provide a cyto-compatible substrate to which cells can attach in vivo and in vitro but are slowly penetrated by cells given the small pore size of the membrane. PCL membranes were produced at a thickness of 0.2 mm and were sterilized by gamma irradiation prior to surgery. The second class of barrier utilized was the commercially available collagen membrane (CM) (Bio-Gide; Geistlich Pharma). These collagen membranes consist of type I and type III collagen and are widely used in surgical procedures to provide a barrier between compartments or to enclose cells in a defined space (eg, in autologous chondrocyte implantation procedures). The membrane is supplied sterilely at a thickness of approximately 1 mm. Both membranes were used as full sheets (PCL and CM) and were fenestrated (fenPCL and fenCM) to allow for improved communication between the progeny and parent compartments. Fenestration was achieved by excising 1.5 mm–diameter segments across each membrane with a sterile biopsy punch (Integra) such that 25% of the scaffold surface was fenestrated and 75% of the scaffold surface remained intact (Figure 1A).

Surgical Methods and Animal Procedures

All animal procedures were approved by the Institutional Animal Care and Use Committee (IACUC; ID 01407) and were performed in accordance with policies set forth by the National Institutes of Health. Bilateral surgery was performed on the stifle joints of 9 male Yucatan minipigs (Sinclair Bioresources). At the time of surgery, animals were 6 months of age and 30 to 35 kg in weight.

Preoperative medication consisted of ketamine (11-33 mg/kg intramuscularly), xylazine (2.2 mg/kg), and cephalexin (250 mg orally). After induction, maintenance of general anesthesia was achieved with isoflurane (1-4 vol%, inhaled), buprenorphine (0.01 mg/kg intramuscularly), and saline (10-20 mL/h intravenously). To access the femoral condyle, an 8 cm–long skin incision over the medial aspect of the patella was made. Soft tissue preparation was followed by a lateral arthrotomy, subluxation of the patella to the medial side, partial resection of the fatpad, and exposure of the lateral aspect of the medial femoral condyle. An osteochondral defect was created using a curved 6.4-mm osteotome (Symmetry Surgical; Hoke). The defect size was 6.4 mm medial to lateral and 9.5 mm anterior to posterior (Figure 1B). The defect was created using orthogonal cuts on the anterior and posterior faces and curved cuts on the medial and lateral faces. The depth was approximately 0.75 cm (Figure 1C). The osteochondral defect (progeny) was removed and either replaced in the defect as a control (ctrl; n = 4) or replaced following interposition of an experimental barrier membrane. Groups included PCL membrane (PCL;

TABLE 1
Study Outline[a]

	Scaffold	Fenestration, %	Thickness, mm
Sham control (n = 5)	None	—	—
No scaffold (n = 4)	None	—	—
PCL (n = 4)	Poly ε-caprolactone	None	0.2
Fenestrated PCL (n = 4)	Poly ε-caprolactone	25	0.2
CM (n = 3)	Collagen	None	1
Fenestrated CM (n = 3)	Collagen	25	1

[a]CM, collagen membrane; PCL, poly(ε-caprolactone).

n = 4), fenestrated PCL membrane (fenPCL; n = 4), a commercially available collagen membrane (CM; n = 3), or fenestrated collagen membrane (fenCM; n = 3) (Table 1). After replacement of the progeny fragment, excess scaffold was trimmed down to the cartilage level (Figure 1, D and E). For all groups, 6 resorbable sutures (6-0 Vicryl; Ethicon) were used to secure the progeny to the defect site (Figure 1E). After soft tissue and skin closure, the incision sites were injected with 5 mL of local anesthetics (bupivacaine; 0.25% solution) per incision.

After extubation and recovery, pigs were allowed full weightbearing status and housed in pairs in pens. Postoperative analgesia consisted of buprenorphine (0.01 mg/kg intramuscularly, twice per day) for the first 3 days postsurgery and carprofen (2-3 mg orally, once per day) for 5 days postsurgery. Cephalexin (250 mg/d orally) was administered until postoperative day 3.

Animals were euthanized on postoperative day 14 after premedication with ketamine (11-33 mg/kg intramuscular) and xylazine (2.2 mg/kg), followed by intravenous overdose of pentobarbital (80 mg/kg) and phenytoin sodium (10 mg/kg). Medial condyles were harvested for further examination. Additionally, 5 lateral condyles (1 per treatment group) were excised and underwent the same analyses, serving as sham controls.

Fluoroscopy and Macroscopic Analysis

Anteroposterior tunnel and lateral fluoroscopic images of each stifle joint were taken intraoperatively, postoperatively, and following euthanasia (Figure 2). After image acquisition (OrthoScan), images were saved, randomized, and blinded for scoring.

At the time of sacrifice, digital photographic images of each defect site were taken following soft tissue dissection. After acquisition, images were saved, randomized, and blinded for scoring.

Micro-CT Analysis

After soft tissue dissection the lateral and medial femoral condyles were separated using a hand saw and fixed in 4% paraformaldehyde (Affymetrix). Lateral condyles served as sham-operated controls (sham). Micro-CT scans for medial condyles and 1 randomly chosen lateral condyle from each treatment group (sham controls) were performed using a VivaCT 75 (Scanco) machine. Specimens were scanned at 55 kVp and 145 μA to image the bone (Figure 2). After scanning, condyles were immersed in Lugol solution (Sigma) for 48 hours and subjected to a second scan to visualize the cartilage and soft tissue. A representative 2-dimensional slice through the midline of each sample was saved separately, randomized, and blinded for scoring. For further analysis, a volume of interest (VOI), represented by a cuboid surrounding the defect, was calculated in each sample. Within each VOI, the bone volume per total volume was computed. Additional full 3-dimensinoal reconstructions of each condyle were generated for visualization purposes.

Histological and Immunohistochemical Analysis

Following micro-CT, condyles were decalcified (Formical-2000; Thermo Fisher Scientific) for 17 days, embedded in paraffin, and cut into 7 μm–thick sections. For each sample, Picrosirius Red (PSR) and Safranin O/Fast Green (Saf-O) staining was performed. Sections were microscopically analyzed for cell and defect morphology and matrix content (collagen and proteoglycan). In addition, immunohistochemistry for collagen types I and II was performed to confirm a fibrous interlayer between progeny and parent bone. For this, sections were deparaffinized, rehydrated, and subjected to proteinase K antigen retrieval for 15 minutes at 37°C. Sections were incubated with either a type II collagen antibody (5 μg/mL) (Developmental Studies Hybridoma Bank, University of Iowa) or a type I collagen antibody (10 μg/mL) (Anti-Collagen type I Antibody, clone 5D8-G9; Millipore) for 1 hour. After washing, signal was detected using the Millipore Immunoperoxidase Secondary Detection System (EMD Millipore Corp). For all stains, images were acquired under brightfield illumination using a Nikon Eclipse NI-E (Nikon) microscope. Images were acquired at a magnification of 10× and stitched using the NIS-Elements AR 4.2 (Nikon) software.

Defect Scoring

To determine which defect group best matched the study goals, a scoring system was implemented based on micro-CT (0-6 points), fluoroscopy (0-2 points), and gross appearance (0-2 points). According to this rubric, lower numbers indicated normal healing while higher numbers indicated an OCD-like appearance (Table 2). An aggregate score in the range of 4 to 7 indicated a stable OCD-like lesion, representative of an ICRS grade 3 OCD lesion. Six blinded reviewers independently scored each sample according this grading scheme.

Statistical Analysis

Statistical analysis was carried out using SPSS (version 20; IBM Corp). For quantitative micro-CT results, a 1-way analysis of variance with Bonferroni post hoc tests was performed. For the OCD score, a Kruskal-Wallis test with Dunn multiple comparison post hoc was used. Significance was set at $P < .05$.

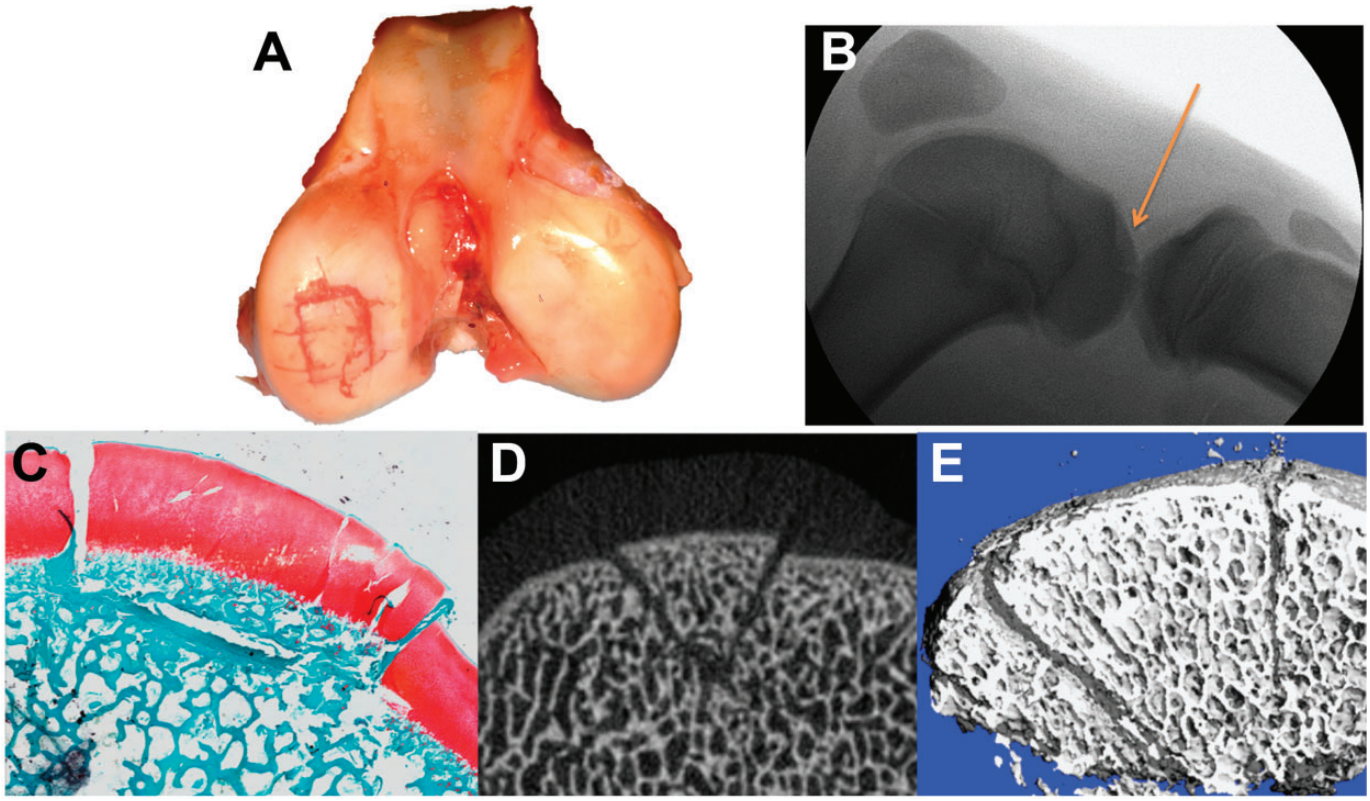

Figure 2. Outcomes and analysis measures. (A) Gross image of left femoral condyles after dissection of soft tissues on the day of surgery. (B) Lateral fluoroscopic postoperative image of the stifle joint. Arrow highlights successful lesion creation. (C) Safranin-O–stained histological section of defect with membrane in place on day 0. (D) Two-dimensional sagittal micro–computed tomography (micro-CT) image of porcine defect with nanofibrous poly(ε-caprolactone) (PCL) membrane at interface on day 0. (E) Three-dimensional micro-CT reconstruction of example defect in a bovine femoral head with PCL membrane in place.

RESULTS

Animal Procedures

All surgeries and postoperative procedures were executed without complication. Animals were weightbearing on all fours on postoperative day 1 and showed no signs of wound or joint infection.

Fluoroscopic and Macroscopic Findings

Preoperative fluoroscopic imaging showed no signs of spontaneous OCD lesions in any animal. All joints were normal and eligible for surgery. Postoperative fluoroscopy demonstrated a clear margin between surgically created progeny and parent bone (Figure 2). After euthanasia at day 14, fluoroscopic appearance of the OCD-like lesion differed between groups. PCL and CM groups showed defined radiolucent regions between progeny and parent bone. The fenPCL and fenCM groups showed a broader range of findings from clear depiction of the progeny to nearly no objective sign of an OCD-like lesion. No lesions could be detected in the control group. In addition, no irregularities were detected in the lateral condyle sham group.

TABLE 2
Categories for the Experimental OCD Score[a]

Category	Points
Micro–computed tomography	
Complete bony consolidation	0
Approximately 2/3 of the cleft shows bony bridging	2
Approximately 1/3 of the cleft shows bony bridging	4
No bony bridging at all	6
Fluoroscopy	
No signs of irregularity at condyle	0
Irregularity, progeny not definable	1
Progeny clearly definable	2
Gross appearance	
Stable, no delamination, even leveled	0
Stable, delamination with or without sunken in progeny	1
Loose body	2

[a]Lower numbers indicate normal healing while higher numbers indicated an osteochondritis dissecans (OCD)–like appearance. An aggregate score of 4-7 indicates a stable OCD-like lesion, representative of an International Cartilage Repair Society grade 3 OCD lesion.

On gross inspection at day 14, the sham group did not show any signs of cartilage deterioration. However, each treatment group showed evidence of the surgical lesion (Figure 3).

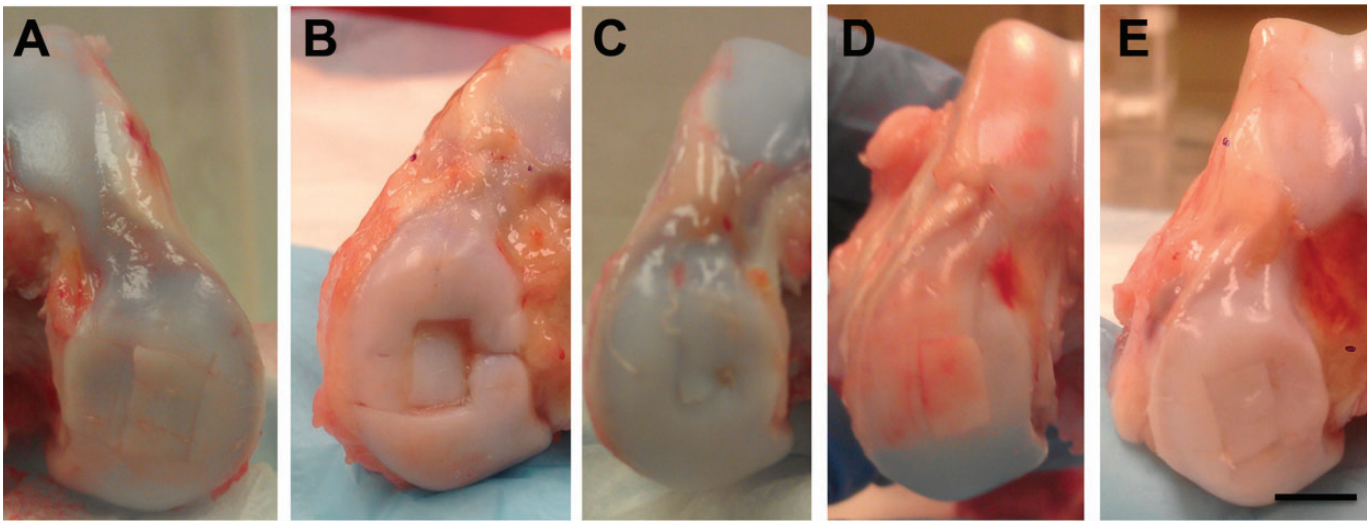

Figure 3. Macroscopic analysis. Representative gross images of the medial femoral condyle from each treatment group 14 days postoperatively. (A) Control group, (B) PCL group, (C) fenPCL group, (D) CM group, and (E) fenCM group. CM, collagen membrane; fenCM, fenestrated CM; fenPCL, fenestrated poly(ε-caprolactone); PCL, poly(ε-caprolactone). Scale bar = 1 cm.

Within the treatment groups, progeny fragments were often depressed in the PCL and CM groups. Both fenPCL and fenCM groups showed variable findings within a given lesion, but overall, progeny fragments did not recess as much as in the nonfenestrated scaffold groups. In the no scaffold group, progeny lesions were flush with the surrounding cartilage, though the cartilage defect margin remained clear.

Micro-CT Findings

Micro-CT imaging revealed that all scaffold-based treatment groups showed bone loss in the space between parent bone and progeny. Bony bridging across >75% of the interface up to complete bony healing was observed only in the control (scaffold-free groups). Occasional bony bridging (<5%) was observed in the fenPCL and fenCM groups. Post-Lugol scans that enabled visualization of the cartilage showed no signs of integration between progeny and parent cartilage in any group. The sham group did not show any signs of abnormal bone or cartilage. Tremendous bone loss was observed in the PCL group and to a notable but lesser degree in the CM group Minimal bone loss was observed in the fenPCL and fenCM groups (Figure 4). Bone loss was observed predominantly in the progeny rather than the parent bone.

Analysis of bone volume per total volume (BV/TV) (Figure 4) in a region of interest inclusive of the defect revealed significant BV loss in the PCL (BV/TV mean ± SD, 27.4% ± 2.3%) group compared with the sham (47.7% ± 1.4%) or no scaffold (54.9% ± 15.1%) groups ($P < .01$ and $P < .05$, respectively). Loss of BV in each of the other surgical groups did not reach statistical significance compared with sham or no scaffold controls (Figure 4H). In addition, a difference in bone loss was evident between the PCL and fenPCL (mean ± SD, BV/TV, 46.6% ± 15.2%) groups ($P < .05$), as well as between the PCL and fenCM (50.9% ± 3.5%) groups ($P < .01$). No other scaffold-based group comparisons revealed significant differences.

Histological Findings

Histological analysis revealed no evidence of parent-progeny cartilage integration in any group (Figure 5). Progeny cartilage stained as intensely for collagen and proteoglycans as did parent cartilage. Inspection of the bony interface showed findings consistent with those seen on micro-CT. Namely, PCL and CM groups showed no signs of bony bridging, and remnants of the scaffold were present. Similar staining of the interface for fibrous tissue was observed in Saf-O and PR sections. That being said, the remaining implanted scaffold layer was much thinner in fenPCL and fenCM groups, and fenestrations were observable in some samples. Parent-progeny bone bridging was evident in the no scaffold groups across nearly the entire interface. Immunostaining showed the interface to stain intensely for collagen I (Col 1) and collagen II (Col 2), supporting the existence of a fibrous interlayer between the progeny and parent bone (Figure 6).

Osteochondritis Dissecans Scoring

To objectively classify the OCD-like nature of the lesions, an OCD score was established (Table 2). Although scoring revealed a difference between no scaffold and scaffold treated groups (control, 2.23 [SD, 1.92]; PCL, 7.58 [SD, 0.50]; fenPCL, 6.35 [SD, 2.12]; CM, 6.81 [SD, 1.06]; fenCM, 5.39 [SD, 2.00]), the only significant differences noted were between the no scaffold and PCL groups ($P < .05$, Figure 7). Taking all outcome measurements into account, fenPCL, CM, and fenCM scaffolds produced OCD-like lesions at postoperative day 14 that most closely resembled the goal of a stable ICRS grade 3 lesion.

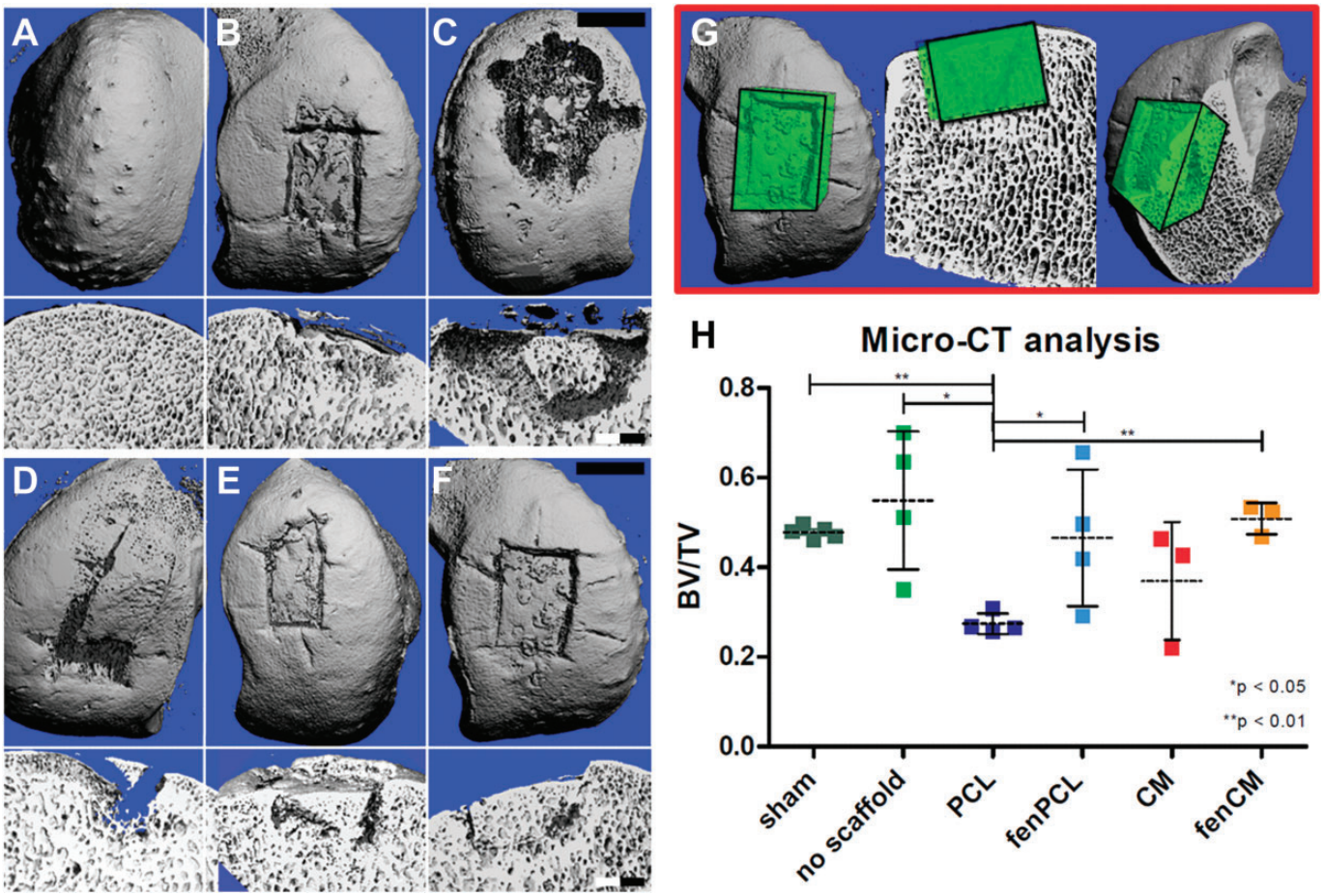

Figure 4. Three-dimensional reconstructions from micro–computed tomography analysis, frontal view (top row; scale, bar = 5 mm) and sagittal view (bottom row; scale bar = 1 mm). (A) Sham, (B) no scaffold, (C) PCL, (D) fenPCL, (E) CM, (F) fenCM. Marked bone loss was observed in the progeny bone for the PCL group. Less remodeling was observed in the fenPCL, CM, and fenCM groups. (G) Schematic showing representative volume of interest (VOI) for quantification of bone volume per total volume (BV/TV). (H) Dot plot showing BV/TV in the VOI for each group. Significant differences were observed between the PCL group and most other groups. *$P < .05$; **$P < .01$. CM, collagen membrane; fenCM, fenestrated CM; fenPCL, fenestrated poly(ε-caprolactone); PCL, poly(ε-caprolactone).

DISCUSSION

While animal models have been instrumental in understanding the etiology of OCD,[9,25,28,41,43] to date, no large animal model exists that can reliably generate OCD-like lesions in terms of size, location, and grade according to ICRS classifications. As such, the potential for animal models to provide a test bed for new surgical interventions is limited. To overcome this, the goal of this pilot study was to engineer OCD-like lesions in a large animal model via biomaterial and surgical intervention. To do so, we created osteochondral lesions on the femoral condyles of the Yucatan minipig and repaired defects with the interposition of membranes of varying degradation characteristics and levels of fenestration. Our hypothesis was that a barrier that could interrupt revascularization and bony healing, while promoting fibrous tissue deposition, might result in the formation of a stable OCD-like lesion.

Results from this pilot study showed osteochondral lesions with hallmarks of OCD at 14 days postoperatively. Consistent with our hypothesis, lesion characteristics depended on the type of barrier material, the degradation characteristics of the barrier, and the degree of fenestration. Specifically, those membranes that were least porous and slowest in their degradation showed notable remodeling of the progeny bone, while those that were more permeable (fenestrated PCL) and more degradable (CM and fenestrated CM) showed resolution toward a stable, fibrous nonunion between the parent and progeny fragment. This finding is reminiscent of an ICRS grade 3 lesion—a stable lesion with a complete discontinuity of the progeny from the parent bone, but with the progeny remaining in situ.[6]

In this study, for all scaffold-treated samples, clefts were evident between the parent bone and progeny fragment, representing one hallmark of OCD. The tissue filling the cleft at this time point was in part newly formed fibrous

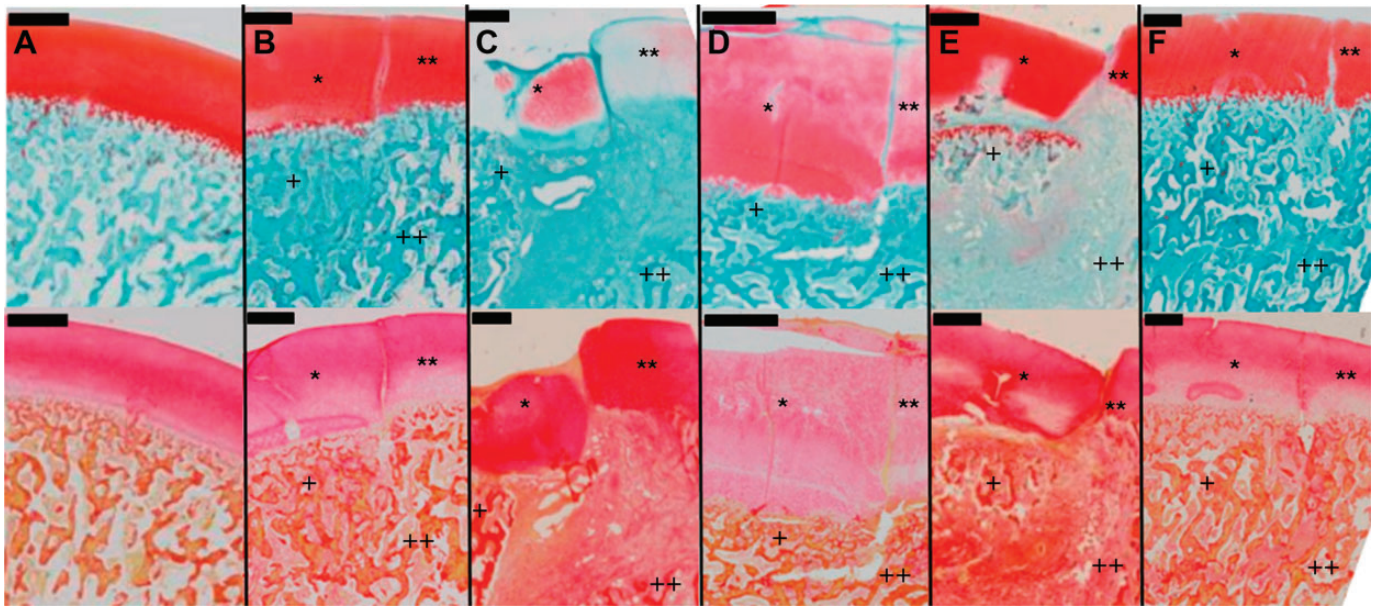

Figure 5. Histological analysis. Safranin-O/Fast Green (top row) and Picrosirius Red (bottom row) staining of representative osteochondritis dissecans–like lesions on day 14. (A) Sham, (B) no scaffold, (C) PCL, (D) fenPCL, (E) CM, and (F) fenCM. *Progeny cartilage; **parent cartilage; $^{+}$progeny bone; $^{++}$parent bone. Fibrous connective tissue is evident at the boundary of all scaffold-containing groups. Scale bar = 1 mm. CM, collagen membrane; fenCM, fenestrated CM; fenPCL, fenestrated poly(ε-caprolactone); PCL, poly(ε-caprolactone).

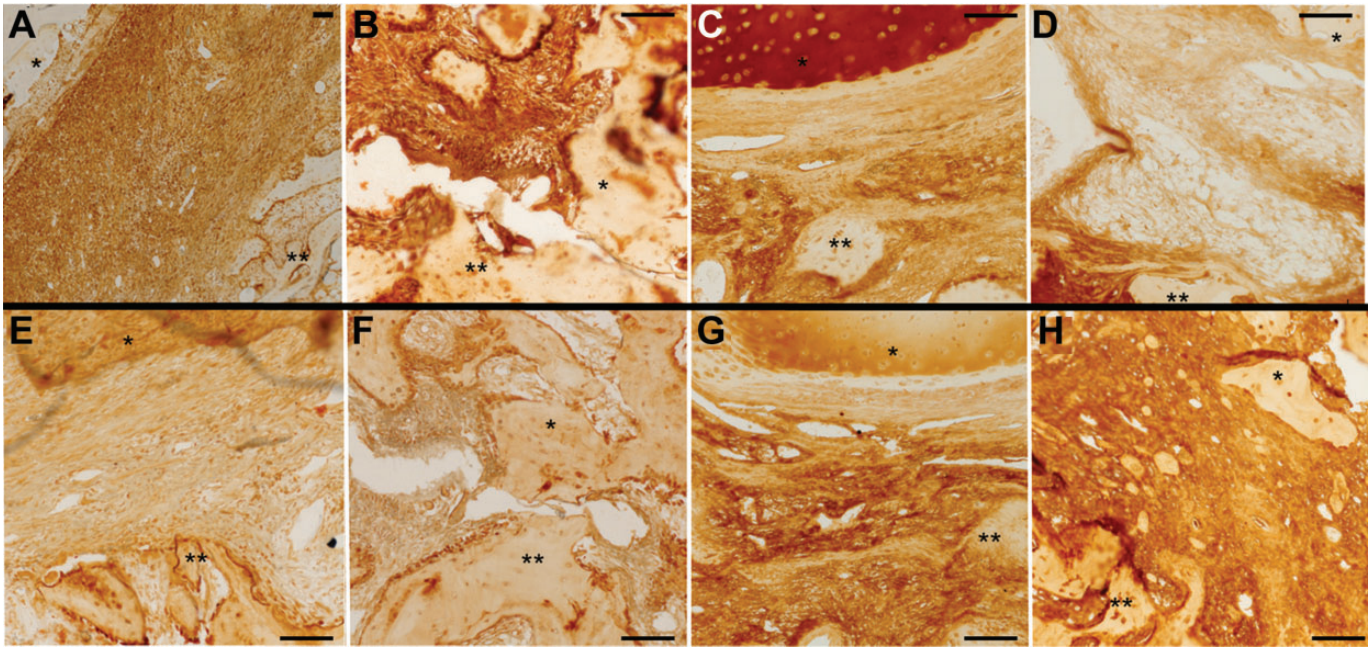

Figure 6. Immunohistochemical analysis. Immunhistochemistry for (A-D) collagen type 2 and (E-H) collagen type 1 at 14 days postoperatively. (A and E) full nanofibrous poly(ε-caprolactone) (PCL) membrane, (B and F) fenestrated PCL, (C and G) full collagen membrane, (D and H) fenestrated collagen membrane. *Progeny bone/cartilage; **parent bone. Scale bar = 100 μm.

tissue and in part remnants of the implanted scaffold. Positive staining for collagen I and II verified the presence of extracellular matrix in the cleft, typical of fibrous tissue, and mimicking the clinical findings in juvenile OCD lesions.[38,40] Besides these morphological similarities, micro-CT and histological findings also suggested that the nature of the barrier between parent bone and progeny correlated with the severity of the defect. Specifically, the least

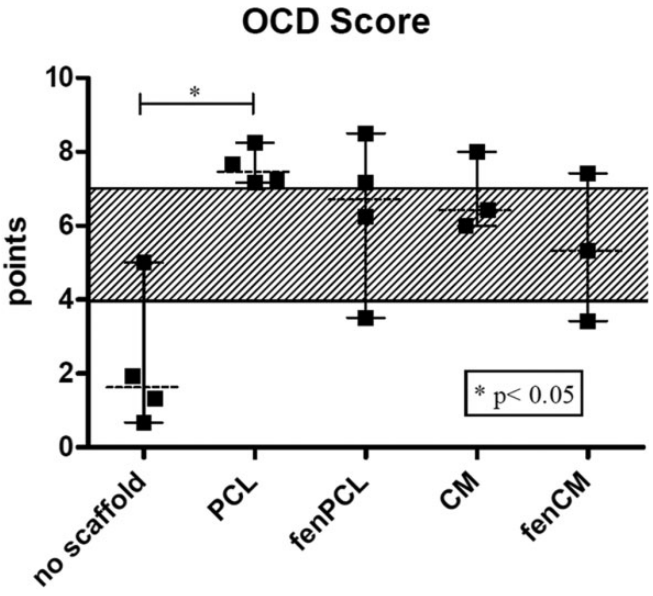

Figure 7. Experimental osteochondritis dissecans (OCD) score. Results of the experimental OCD score with the striped region depicting the target score between 4 and 7, which mirrors a lesion severity according to International Cartilage Repair Society grade 3. Three of the scaffold-treated groups matched the target region. CM, collagen membrane; fenCM, fenestrated CM; fenPCL, fenestrated poly(ε-caprolactone); PCL, poly(ε-caprolactone).

permeable formulation (PCL) generated a marked remodeling response in the progeny bone, and this could be attenuated by introducing fenestrations that likely enhanced vascular access. Shea et al[34] reported in a review on histological findings in OCD lesions that 7 of 11 studies have shown necrosis of the subchondral bone in the progeny fragment. Recent studies suggest that this may be due to limited nutrient supply. Of note, lesions in the control group (without placement of a barrier) showed nearly complete bony healing at postoperative day 14. Thus, the degree and duration of time that the barrier prevents revascularization of the progeny fragment may be used to tune the severity of the developed lesion, and perhaps its permanency.

A number of clinically relevant outcomes were used in this study to assess defects. Imaging by fluoroscopy showed typical signs of OCD in all scaffold-treated groups. Current clinical recommendations suggest the use of plain radiographs in patients presenting with knee pain, whereas the recommendation for magnetic resonance imaging (MRI) following positive radiographs is still inconclusive.[10] In our study, micro-CT imaging showed differential bone resorption as a function of treatment group and proved to be a sensitive metric by which to judge differences between groups. While micro-CT is only feasible in samples ex vivo, clinical studies using MRI to visualize bone microarchitecture[39] could provide similar resolution in humans. This would also allow for better comparison with clinics, as radiographs and MRI are currently the most commonly used imaging modalities in OCD.[10,14] On the other hand, a recent study showed the 100% predictive value of CT scans in the diagnosis of early stages of osteochondrosis in the distal femur of young piglets,[29] and so this imaging modality should be pursued as well. Additionally, angiographic methods would be useful for assessing whether the subchondral bone vascularity was indeed perturbed by the barrier.

While the results of this study show promise toward the creation of OCD-like lesions in the Yucatan minipig, several limitations are evident. First, we only examined lesions over the short term (at 2 weeks postoperatively). This time point was chosen given the pilot nature of the study, as well as to rule out certain barrier formulations that were clearly ineffective at creating stable nonunions. While it will be important to chart the progression of the formed lesions over time, it is important to note that studies focused on the effect of disturbance of the blood supply use similar time points to understand underlying etiology.[9,28,37,43] Furthermore, while we used several clinically relevant outcomes, we did not employ the common clinical procedure in which the lesion is probed for stability by placing a hook in the cleft and trying to open the gap.[20] This was not performed as further evaluation of the sample by micro-CT and histology would have been at risk. An additional limitation of the study was the age of the animals used. Most OCD studies, including ours, use skeletally immature animals. Studies investigating the underlying etiology aim to mimic as closely as possible the age of disease onset, which may occur as early as in utero.[25] In our study, we used comparatively older but still skeletally immature animals. As the intention of the study was to create a clinically relevant animal model of OCD to study current and future treatment options, we matched the age of the animals to that of the highest prevalence of OCD in humans (between 10 and 16 years[12,21]), when growth plates are still open and skeletal growth is still occurring.

Despite these acknowledged limitations, data from this study show clear evidence of the successful creation of an OCD-like lesion in the knee of the Yucatan minipig. Having established this platform, this work may serve as a reliable model with which to further investigate the natural disease course as well as treatment options for human OCD. In future longer term studies, it will be important to carefully investigate how the artificial barriers influence the progression of disease and to perhaps tune these attributes to produce the most appropriate lesion for different clinical scenarios by varying the temporal characteristics of the barrier. This could be readily achieved via modulations in the degree of fenestration or by choosing polymers with different degradation rates. Alternatively, scaffold could be seeded with a fibrous cell type (such as a dermal or tendon fibroblast) to promote nonunion via fibrous extracellular matrix production at the interface. Furthermore, while animals in this study were allowed free cage activity after surgery, postsurgical rehabilitation regimens could be assayed to either promote resolution (by limiting motion) or to promote OCD lesion progression (by subjecting animals to treadmill exercise so that the defects see regular micromotion). Taken together, these data point to the successful creation of an osteochondral lesion in the Yucatan minipig that mirrors that of an ICRS

grade 3 OCD lesion in humans and set the stage for ongoing model refinement as well as exploration of novel interventional therapies to restore function and bone and cartilage patency in individuals affected by this rare but significant disease.

REFERENCES

1. Ahern BJ, Parvizi J, Boston R, Schaer TP. Preclinical animal models in single site cartilage defect testing: a systematic review. *Osteoarthritis Cartilage*. 2009;17:705-713.
2. Aichroth P. Osteochondritis dissecans of the knee. A clinical survey. *J Bone Joint Surg Br*. 1971;53:440-447.
3. Barrie HJ. Osteochondritis dissecans 1887-1987. A centennial look at König's memorable phrase. *J Bone Joint Surg Br*. 1987;69:693-695.
4. Bradley J, Dandy DJ. Results of drilling osteochondritis dissecans before skeletal maturity. *J Bone Joint Surg Br*. 1989;71:642-644.
5. Bravo C, Kawamura H, Yamaguchi T, Hotokebuchi T, Sugioka Y. Experimental osteochondritis dissecans—the role of cartilage canals in chondral fractures of young rabbits. *Hukuoka Acta Med*. 1996;87: 133-141.
6. Brittberg M, Winalski CS. Evaluation of cartilage injuries and repair. *J Bone Joint Surg Am*. 2003;85(suppl 2):58-69.
7. Bruns J, Rosenbach B, Kahrs J. Etiopathogenetic aspects of medial osteochondrosis dissecans tali [in German]. *Sportverletz Sportschaden*. 1992;6:43-49.
8. Cahill BR. Osteochondritis dissecans of the knee: treatment of juvenile and adult forms. *J Am Acad Orthop Surg*. 1995;3:237-247.
9. Carlson CS, Meuten DJ, Richardson DC. Ischemic necrosis of cartilage in spontaneous and experimental lesions of osteochondrosis. *J Orthop Res*. 1991;9:317-329.
10. Chambers HG, Shea KG, Anderson AF, et al. American Academy of Orthopaedic Surgeons clinical practice guideline on: the diagnosis and treatment of osteochondritis dissecans. *J Bone Joint Surg Am*. 2012;94:1322-1324.
11. Chu CR, Szczodry M, Bruno S. Animal models for cartilage regeneration and repair. *Tissue Eng Part B Rev*. 2010;16:105-115.
12. Crawford DC, Safran MR. Osteochondritis dissecans of the knee. *J Am Acad Orthop Surg*. 2006;14:90-100.
13. Edmonds EW, Albright J, Bastrom T, Chambers HG. Outcomes of extra-articular, intra-epiphyseal drilling for osteochondritis dissecans of the knee. *J Pediatr Orthop*. 2010;30:870-878.
14. Edmonds EW, Polousky J. A review of knowledge in osteochondritis dissecans: 123 years of minimal evolution from König to the ROCK Study Group. *Clin Orthop Relat Res*. 2013;471:1118-1126.
15. Green WT, Banks HH. Osteochondritis dissecans in children. 1952. *Clin Orthop Relat Res*. 1990;(255):3-12.
16. Grondalen T. Osteochondrosis and arthrosis in pigs. *Acta Vet Scand*. 1974;15:1-25.
17. Gunton MJ, Carey JL, Shaw CR, Murnaghan ML. Drilling juvenile osteochondritis dissecans: retro- or transarticular? *Clin Orthop Relat Res*. 2013;471:1144-1151.
18. Hefti F, Beguiristain J, Krauspe R, et al. Osteochondritis dissecans: a multicenter study of the European Pediatric Orthopedic Society. *J Pediatr Orthop Part B*. 1999;8:231-245.
19. Jacobi M, Wahl P, Bouaicha S, Jakob RP, Gautier E. Association between mechanical axis of the leg and osteochondritis dissecans of the knee: radiographic study on 103 knees. *Am J Sports Med*. 2010;38:1425-1428.
20. Jacobs JC Jr, Archibald-Seiffer N, Grimm NL, Carey JL, Shea KG. A review of arthroscopic classification systems for osteochondritis dissecans of the knee. *Clin Sports Med*. 2014;33:189-197.
21. Kessler JI, Nikizad H, Shea KG, Jacobs JC Jr, Bebchuk JD, Weiss JM. The demographics and epidemiology of osteochondritis dissecans of the knee in children and adolescents. *Am J Sports Med*. 2014;42: 320-326.
22. König F. About free body in the joints [in German]. *Zeitschr Chir*. 1888; 27:90-109.
23. Linden B. Osteochondritis dissecans of the femoral condyles: a long-term follow-up study. *J Bone Joint Surg Am*. 1977;59:769-776.
24. Lyon R, Liu X, Kubin M, Schwab J. Does extracorporeal shock wave therapy enhance healing of osteochondritis dissecans of the rabbit knee? *Clin Orthop Relat Res*. 2013;471:1159-1165.
25. McCoy AM, Toth F, Dolvik NI, et al. Articular osteochondrosis: a comparison of naturally-occuring human and animal disease. *Osteoarthritis Cartilage*. 2013;21:1638-1647.
26. Milgram JW. Radiological and pathological manifestations of osteochondritis dissecans of the distal femur. A study of 50 cases. *Radiology*. 1978;126:305-311.
27. Nagura S. Osteochondritis dissecans of the hip joint and its etiology [in German]. *Arch Orthop Unfallchir*. 1969;65:371-374.
28. Olstad K, Hendrickson EH, Carlson CS, Ekman S, Dolvik NI. Transection of vessels in epiphyseal cartilage canals leads to osteochondrosis and osteochondrosis dissecans in the femoro-patellar joint of foals; a potential model of juvenile osteochondritis dissecans. *Osteoarthritis Cartilage*. 2013;21:730-738.
29. Olstad K, Kongsro J, Eli Grindflek E, Dolvik NI. Ossification defects detected in CT scans represent early osteochondrosis in the distal femur of piglets. *J Orthop Res*. 2014;32:1014-1023.
30. Olstad K, Ytrehus B, Ekman S, Carlson CS, Dolvik NI. Early lesions of osteochondrosis in the distal tibia of foals. *J Orthop Res*. 2007;25: 1094-1105.
31. Phillips HO, Grubb SA. Familial multiple osteochondritis dissecans. Report of a kindred. *J Bone Joint Surg Am*. 1985;67:155-156.
32. Polousky JD. Juvenile osteochondritis dissecans. *Sports Med Arthrosc*. 2011;19:56-63.
33. Rangkasenee N, Murani E, Brunner RM, et al. Genome-wide association identifiesTBX5 as candidate gene for osteochondrosis providing a functional link to cartilage perfusion as initial factor. *Front Genet*. 2013; 4:78.
34. Shea KG, Jacobs JC Jr, Carey JL, Anderson AF, Oxford JT. Osteochondritis dissecans knee histology studies have variable findings and theories of etiology. *Clin Orthop Relat Res*. 2013; 471:1127-1136.
35. Shea KG, Jacobs JC Jr, Grimm NL, Pfeiffer RP. Osteochondritis dissecans development after bone contusion of the knee in the skeletally immature: a case series. *Knee Surg Sports Traumatol Arthrosc*. 2013; 21:403-407.
36. Stattin EL, Wiklund F, Lindblom K, et al. A missense mutation in the aggrecan C-type lectin domain disrupts extracellular matrix interactions and causes dominant familial osteochondritis dissecans. *Am J Hum Genet*. 2010;86:126-137.
37. Toth F, Nissi MJ, Zhang J, et al. Histological confirmation and biological significance of cartilage canals demonstrated using high field MRI in swine at predilection sites of osteochondrosis. *J Orthop Res*. 2013;31:2006-2012.
38. Uozumi H, Sugita T, Aizawa T, Takahashi A, Ohnuma M, Itoi E. Histologic findings and possible causes of osteochondritis dissecans of the knee. *Am J Sports Med*. 2009;37:2003-2008.
39. Wehrli F. Magnetic resonance of calcified tissues. *J Magn Reson*. 2013;229:35-48.
40. Yonetani Y, Nakamura N, Natsuume T, Shiozaki Y, Tanaka Y, Horibe S. Histological evaluation of juvenile osteochondritis dissecans of the knee: a case series. *Knee Surg Sports Traumatol Arthrosc*. 2010;18: 723-730.
41. Ytrehus B, Ekman S, Carlson CS, Teige J, Reinholt FP. Focal changes of blood supply during normal epiphyseal growth are central in the pathogenesis of osteochondrosis in pigs. *Bone*. 2004;35: 1294-1306.
42. Ytrehus B, Grindflek E, Teige J, et al. The effect of parentage on the prevalence, severity and location of lesions of osteochondrosis in swine. *J Vet Med A Physiol Pathol Clin Med*. 2004;51:188-195.
43. Ytrehus B, Haga HA, Mellum CN, et al. Experimental ischemia of porcine growth cartilage produces lesions of osteochondrosis. *J Orthop Res*. 2004;22:1201-1209.